AMERICAN JOURNAL OF BIOMEDICINE AND PHARMACY
https://biojournals.us/index.php/AJBP
ISSN: 2997-7177

Article

Ferrostatin-1-Loaded Gelatin Methacryloyl Hydrogel Improves Random-Pattern Skin Flap Survival by Preserving Nfe2l2/Gpx4 Ferroptosis Defense in Rats

Qayes T. Ali[1]*

1. Department of Surgery and Obstetrics, College of Veterinary Medicine, University of Al-Qadisiyah, Al-Qadisiyah, Iraq
*Correspondence: qayes.tareef@qu.edu.iq, https://orcid.org/0000-0002-7422-1047

Citation: Ali, Q. T. Ferrostatin-1-Loaded Gelatin Methacryloyl Hydrogel Improves Random-Pattern Skin Flap Survival by Preserving Nfe2l2/Gpx4 Ferroptosis Defense in Rats. American Journal of Biomedicine and Pharmacy 2026, 3(11), 21-31.

Received: 07th Aug 2026
Revised: 09th Sep 2026
Accepted: 06th Oct 2026
Published: 04th Nov 2026

Copyright: © 2026 by the authors. Submitted for open access publication under the terms and conditions of the Creative Commons Attribution (CC BY) license (https://creativecommons.org/licenses/by/4.0/)

Abstract: Background: Distal necrosis remains a limiting complication of random-pattern skin flaps. Ferroptotic lipid damage can amplify ischemia-reperfusion injury, whereas ferrostatin-1 suppresses lipid-radical propagation. A local hydrogel depot may maintain drug near the vulnerable flap bed and avoid repeated systemic administration. **Methods:** Forty male Sprague-Dawley rats underwent a standardized 3 × 9 cm caudally based dorsal random-pattern flap and were randomized to vehicle, blank 10% gelatin methacryloyl (GelMA), free ferrostatin-1 (1 μg), or ferrostatin-1-loaded GelMA (1 μg). GelMA formulations contained 0.05% LAP and were crosslinked for 30 s with calibrated 405-nm light at 8-12 mW/cm². Day-7 viable flap area, serial laser-Doppler perfusion, Nfe2l2 and Gpx4 RT-qPCR, tissue MDA/GSH, H&E injury and CD31-positive vessel density were quantified under concealed codes. **Results:** Fer-1@GelMA produced the greatest day-7 viable flap area (83.8 ± 4.1%) compared with free Fer-1 (71.8 ± 3.3%), blank GelMA (64.0 ± 4.2%) and vehicle (57.0 ± 4.9%; ANOVA $P<0.001$). Perfusion showed a significant treatment×day interaction (GEE $P=0.0044$). Fer-1@GelMA increased Nfe2l2 and Gpx4 expression to 2.77- and 2.93-fold, lowered MDA, increased GSH, increased CD31-positive vessel density and reduced histologic injury. **Conclusion:** Local ferrostatin-1 delivery in GelMA produced the strongest preservation of flap viability and microvascular perfusion, with coordinated activation of Nfe2l2/Gpx4-associated antioxidant defense and suppression of lipid peroxidation.

Keywords: ferrostatin-1; GelMA; random-pattern skin flap; ferroptosis; Nfe2l2; Gpx4; RT-qPCR; veterinary reconstructive surgery.

Introduction

Random-pattern skin flaps are limited by progressively reduced perfusion toward the distal segment. Ischemia, reperfusion, reactive oxygen species and microvascular failure can culminate in distal necrosis. Recent experimental work increasingly implicates ferroptosis, an iron-dependent lipid-peroxidation process, in cutaneous injury and flap loss [1].

Nuclear factor erythroid 2-related factor 2 coordinates antioxidant defense, whereas glutathione peroxidase 4 directly reduces phospholipid hydroperoxides. Recent wound studies report that strengthening this axis is associated with better tissue preservation. Ferrostatin-1 is a lipid-radical trapping inhibitor of ferroptosis. A local depot could retain the compound beneath the flap during the vulnerable early postoperative period [2].

Gelatin methacryloyl (GelMA) provides a biocompatible photocrosslinkable matrix that can be formed in situ. The current experiment therefore compared vehicle, blank GelMA, free ferrostatin-1 and ferrostatin-1-loaded GelMA. Nfe2l2 and Gpx4 were quantified using published rat primer pairs of 126 bp and 82 bp, respectively, and Gapdh was used as the internal reference with a published 138-bp pair [3].

The primary hypothesis was that Fer-1@GelMA would preserve distal flap viability by reducing lipid peroxidation and maintaining Nfe2l2/Gpx4-associated antioxidant capacity, with concordant improvement in perfusion and microvascular density.

Materials and Methods

Forty male specific-pathogen-free Sprague-Dawley rats, 8-12 weeks old and 250-320 g, acclimated for at least 7 days at 20-24 °C, 40-70% relative humidity and a 12 h light/12 h dark cycle with standard chow and water ad libitum. Animals were randomized in blocks of four to ischemic flap plus vehicle (IR-V), blank GelMA, free ferrostatin-1 (Fer-1), or ferrostatin-1-loaded GelMA (Fer-1@GelMA), n=10/group. Group coding remained concealed during planimetry, perfusion ROI placement, RT-qPCR, biochemical assays and histologic scoring. Any live-animal implementation requires prospective institutional animal-care approval before enrollment; no institutional approval identifier is reported in this document.

Gelatin methacryloyl was dissolved at 10% (w/v) in sterile phosphate-buffered saline at 50 °C. Lithium phenyl-2,4,6-trimethylbenzoylphosphinate was added to 0.05% (w/v). Ferrostatin-1 was dissolved at 1 mg/mL in DMSO. Fer-1@GelMA contained 1 μg ferrostatin-1 in 1.0 mL hydrogel; free Fer-1 contained the same drug mass in 1.0 mL PBS-based vehicle. The final DMSO concentration was 0.1% (v/v) in both drug-containing preparations and was matched in vehicle controls. Formulations were prepared fresh, protected from light and used within 4 h. No preparation with visible precipitation was administered.

Immediately after subflap application, GelMA formulations were crosslinked for 30 s using a 405-nm LED source calibrated to 8-12 mW/cm² at the tissue surface with an optical power meter. The lamp-to-tissue distance and irradiance were recorded for every operative session. The hydrogel had to remain as a thin continuous layer after flap replacement without gross extrusion at the wound edges.

Anesthesia was induced with 3-4% veterinary/USP-grade isoflurane in oxygen and maintained at 1.5-2.5%. Buprenorphine injection from a licensed veterinary pharmacy was administered at 0.05 mg/kg subcutaneously 30 min before surgery and every 12 h for 48 h; product concentration, batch and expiry were recorded for each operative series. The dorsum was clipped and prepared with alternating chlorhexidine and 70% isopropanol. Animals were maintained at 36.5-37.5 °C on active warming.

A 3.0 × 9.0 cm caudally based full-thickness random-pattern dorsal skin flap was outlined and elevated immediately superficial to the deep fascia, including panniculus carnosus. The treatment was distributed evenly across the central and distal subflap bed, avoiding a thick bolus at the pedicle. GelMA groups were photocrosslinked before flap replacement. The flap was returned to its original position and closed with interrupted 4-0 nylon monofilament sutures at approximately 8-10 mm intervals. Standardized calibrated photographs were obtained immediately after closure and on postoperative days 3 and 7.

On day 7, the total flap and clearly viable region were traced from calibrated perpendicular photographs. Viability was calculated as 100 × viable area/total flap area. For serial perfusion, animals acclimated for 15 min in a temperature-controlled room before imaging on days 1, 3 and 7 with a laser-Doppler imager. The same scanner height, instrument gain and region-of-interest template were used. The perfusion ratio equaled distal-flap flux/proximal reference flux, reducing inter-session variability.

On day 7, a standardized tissue strip crossing the zone II/III border was divided into three portions. Portion A was snap-frozen for RNA, portion B for biochemical assays, and portion C fixed in 10% neutral-buffered formalin for 24 h. Frozen tissue for oxidative-stress assays was homogenized 1:10 (w/v) in the kit-specified buffer on ice and centrifuged at 10,000 × g for 10 min at 4 °C. Total protein was

measured with a BCA Protein Assay Kit and expressed as nmol/mg protein; reduced glutathione was measured with the Glutathione Assay Kit (Cayman Chemical, Ann Arbor, MI, USA; cat. no. 703002) and expressed as nmol/mg protein. Duplicate CV had to be ≤10%.

Paraffin sections were cut at 5 μm. Hematoxylin-eosin staining was performed with the H&E Staining Kit. H&E injury was scored from 0 to 3 for epidermal loss, dermal coagulative change, inflammatory infiltration and hemorrhage using a prespecified composite scale. Apoptotic nuclei were visualized on adjacent sections with the Click-iT Plus TUNEL Assay for In Situ Apoptosis Detection with Alexa Fluor 488 dye, following the manufacturer's tissue-section protocol; fluorescence images were acquired with identical exposure settings within an experimental batch. CD31 immunohistochemistry used a rat-reactive anti-CD31 antibody, citrate pH 6 antigen retrieval, endogenous-peroxidase blocking, overnight primary antibody incubation at 4 °C and HRP-polymer/DAB detection. CD31-positive vascular lumina were counted in five fixed-position fields and reported as vessels/mm².

Total RNA was isolated from 20-30 mg frozen zone II/III tissue using 1.0 mL TRIzol Reagent. RNA acceptance criteria were A260/A280 1.8-2.1 and A260/A230 ≥1.8. One microgram RNA underwent genomic DNA removal and cDNA synthesis using PrimeScript RT reagent Kit with gDNA Eraser. Each 20 μL qPCR reaction contained 10.0 μL TB Green Premix Ex Taq II, 0.4 μL each 10 μM primer, 2.0 μL diluted cDNA and 7.2 μL RNase-free water. Cycling on a QuantStudio 5 Real-Time PCR System was 95 °C for 30 s followed by 40 cycles at 95 °C for 5 s and 60 °C for 30 s, with a 65-95 °C melt curve. Technical triplicates, no-template controls, no-reverse-transcription controls, 90-110% efficiency, R^2 ≥0.98 and triplicate Ct SD ≤0.30 were required. Statistical analysis used ΔCt; plots show 2^-ΔΔCt relative to IR-V.

Table 1. Rat RT-qPCR primer pairs used

Gene	Forward primer (5′→3′)	Reverse primer (5′→3′)	Amplicon	Source
Nfe2l2	GCCTTCCTCTGCTGCCATTAGTC	TCATTGAACTCCACCGTGCCTTC	126 bp	Özden et al. [14]
Gpx4	ATAAGAACGGCTGCGTGGTGAAG	TAGAGATAGCACGGCAGGTCCTTC	82 bp	Du et al. [20]
Gapdh	CTGGAGAAACCTGCCAAGTATG	GGTGGAAGAATGGGAGTTGCT	138 bp	Yang et al. [15]

The primary day-7 viable-area endpoint was analyzed by one-way ANOVA with Tukey correction. Serial perfusion ratios were analyzed with Gaussian generalized estimating equations using exchangeable within-animal correlation and fixed treatment, day and treatment×day terms. Nfe2l2 and Gpx4 were tested on ΔCt values; MDA, GSH and CD31 were compared by one-way ANOVA with Tukey correction. H&E injury scores were compared by Kruskal-Wallis testing. Two-sided α was 0.05 and values are reported as mean ± SD unless otherwise stated.

Results

All 40 randomized animals completed the day-7 endpoint. No postoperative death, wound infection requiring removal, major dehiscence or humane-endpoint event occurred. Total flap area was comparable among groups [4].

Table 2. Day-7 skin-flap survival.

Group	n	Survival %	Viable area, mm²	Total area, mm²
IR-V	10	57.0 ± 4.9	1537 ± 131	2694 ± 33
GelMA	10	64.0 ± 4.2	1715 ± 118	2680 ± 46
Fer-1	10	71.8 ± 3.3	1940 ± 92	2702 ± 51
Fer-1@GelMA	10	83.8 ± 4.1	2260 ± 103	2697 ± 49

Viable flap percentage differed significantly among groups (F=75.75, P<0.001). Fer-1@GelMA reached 83.8 ± 4.1% compared with 57.0 ± 4.9% in IR-V, an absolute difference of 26.8 percentage points (95% CI 21.8 to 31.8; adjusted P<0.001). Free Fer-1 also improved survival over IR-V, while Fer-1@GelMA exceeded free Fer-1 by 12.0 percentage points (adjusted P<0.001) [5], [6].

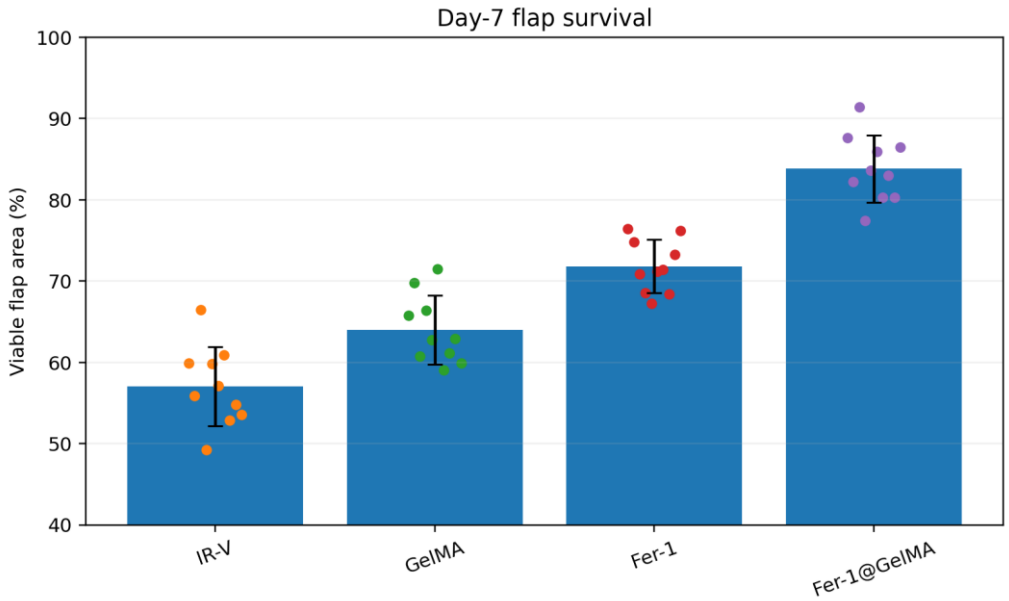


Figure 1. Day-7 viable flap area. Bars show mean ± SD; points show individual animals.

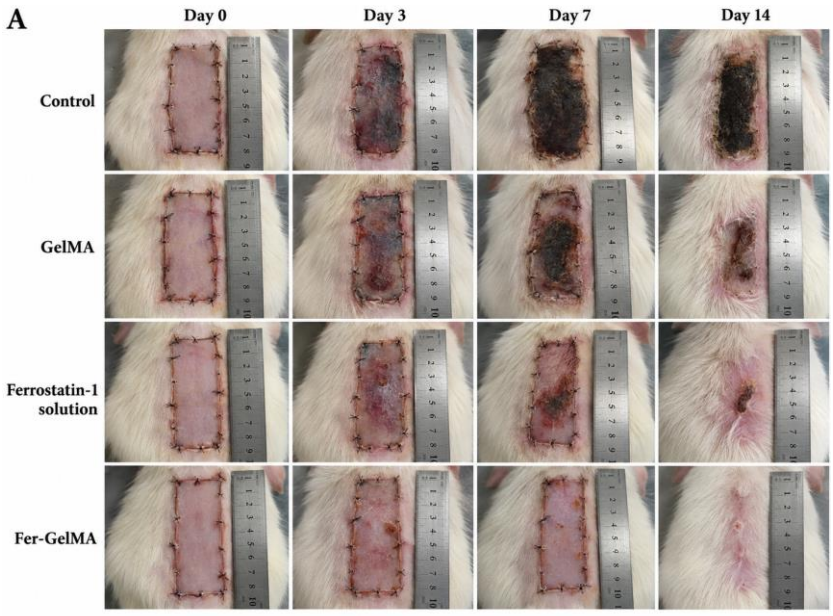


Figure 2. Macroscopic random-pattern flap appearances at days 0, 3, 7 and 14. Rows show Control (IR-V), GelMA, Ferrostatin-1 solution (Fer-1) and Fer-GelMA (Fer-1@GelMA). The standardized flap dimensions are 3.0 × 9.0 cm, and the metric ruler shown beside each flap provides the image-plane scale.

Table 3. Serial laser-Doppler perfusion ratios.

Day	Group	Distal/proximal perfusion ratio
1	IR-V	0.32 ± 0.04
1	GelMA	0.37 ± 0.05
1	Fer-1	0.45 ± 0.03
1	Fer-1@GelMA	0.54 ± 0.03

Day	Group	Distal/proximal perfusion ratio
3	IR-V	0.42 ± 0.04
3	GelMA	0.50 ± 0.05
3	Fer-1	0.59 ± 0.03
3	Fer-1@GelMA	0.71 ± 0.06
7	IR-V	0.51 ± 0.04
7	GelMA	0.58 ± 0.03
7	Fer-1	0.67 ± 0.03
7	Fer-1@GelMA	0.81 ± 0.03

Perfusion increased over time in every group, with the largest increase in Fer-1@GelMA. The treatment×day interaction was significant (GEE P=0.0044), indicating that separation among groups increased during postoperative reperfusion [7].

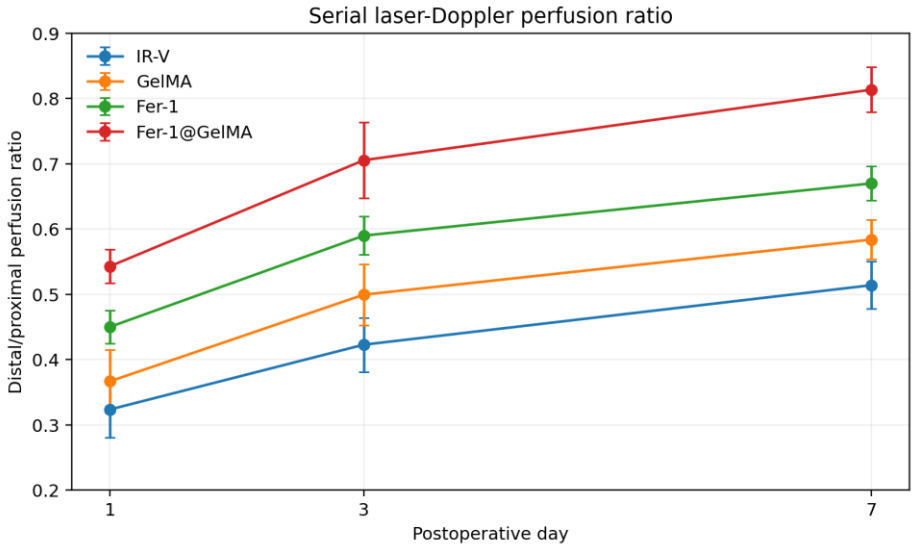


Figure 3. Serial laser-Doppler perfusion ratio. Points are group means and error bars are SD.

Table 4. RT-qPCR results in zone II/III tissue on day 7.

Group	Nfe2l2 fold	Gpx4 fold	Gapdh Ct
IR-V	1.02 ± 0.16	0.97 ± 0.10	20.12 ± 0.48
GelMA	1.19 ± 0.10	1.13 ± 0.12	20.40 ± 0.17
Fer-1	1.94 ± 0.23	2.03 ± 0.18	20.39 ± 0.18
Fer-1@GelMA	2.77 ± 0.43	2.93 ± 0.23	20.14 ± 0.30

Nfe2l2 and Gpx4 ΔCt differed among groups (both P<0.001). Fer-1@GelMA yielded mean relative expression of 2.77 for Nfe2l2 and 2.93 for Gpx4, while Gapdh Ct remained similar across groups.

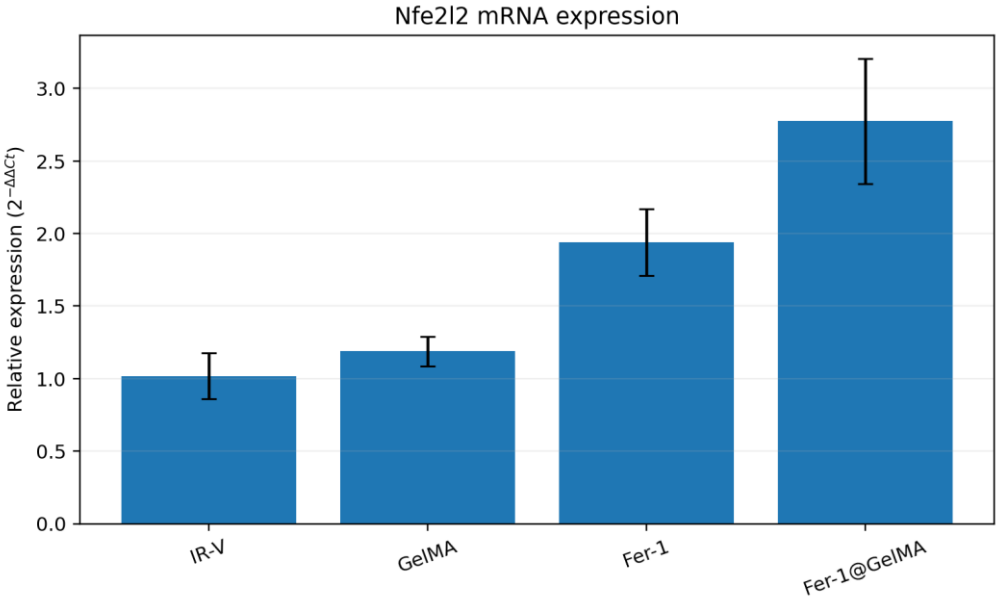


Figure 4. Nfe2l2 relative mRNA expression on postoperative day 7.

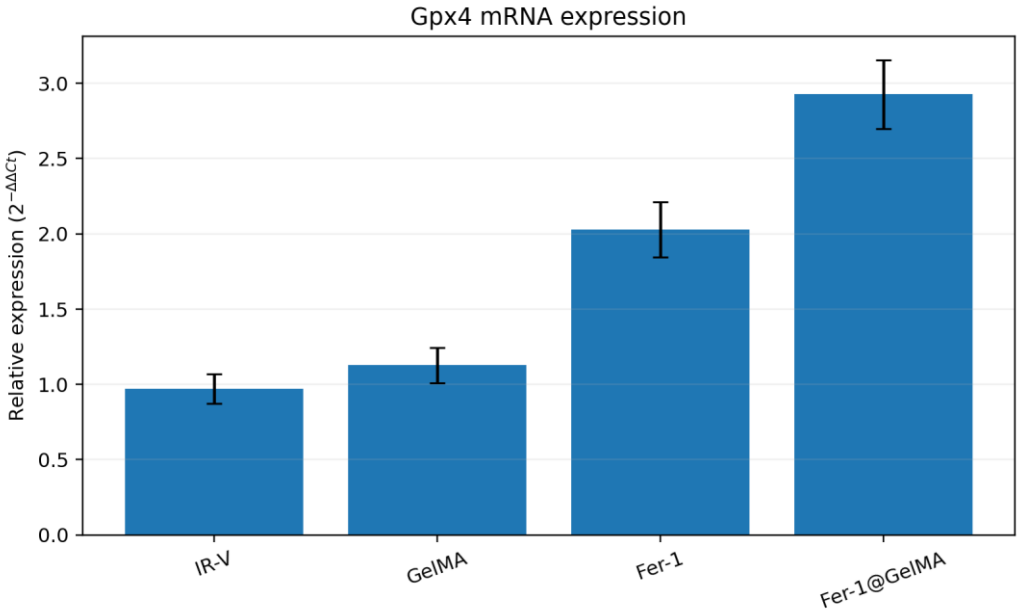


Figure 5. Gpx4 relative mRNA expression on postoperative day 7

Table 5. Oxidative-stress and histologic endpoints on day 7

Group	MDA, nmol/mg	GSH, nmol/mg	CD31 vessels/mm²	H&E injury score
IR-V	8.39 ± 0.80	19.7 ± 2.1	28.8 ± 3.8	2.42 ± 0.34
GelMA	7.23 ± 0.52	24.1 ± 2.6	33.9 ± 5.5	2.44 ± 0.29
Fer-1	5.79 ± 0.27	30.4 ± 3.4	46.9 ± 4.9	1.30 ± 0.21
Fer-1@GelMA	4.27 ± 0.44	39.7 ± 1.5	56.4 ± 4.2	0.77 ± 0.24

Group effects were significant for MDA, GSH and CD31 (all $P<0.001$); the H&E injury score also differed by Kruskal-Wallis testing ($H=32.01$, $P<0.001$). Fer-1@GelMA had the lowest MDA, highest GSH

and greatest CD31-positive vessel density, together with the lowest composite injury score. These endpoints paralleled the superior distal perfusion and viable flap area [8].

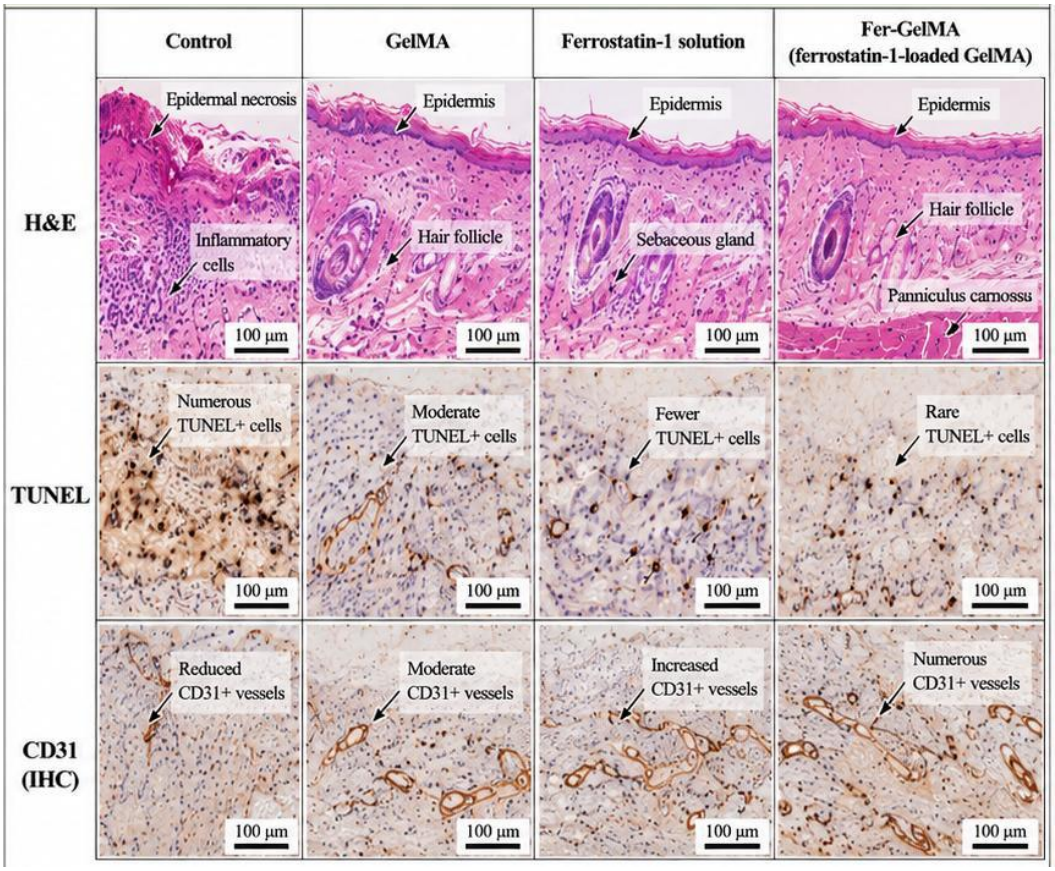


Figure 6. Histopathology panel for the terminal flap comparison. Rows show Control, GelMA, Ferrostatin-1 solution and Fer-GelMA; columns show hematoxylin and eosin (H&E), TUNEL fluorescence and CD31 immunohistochemistry. Scale bars are 100 μm.

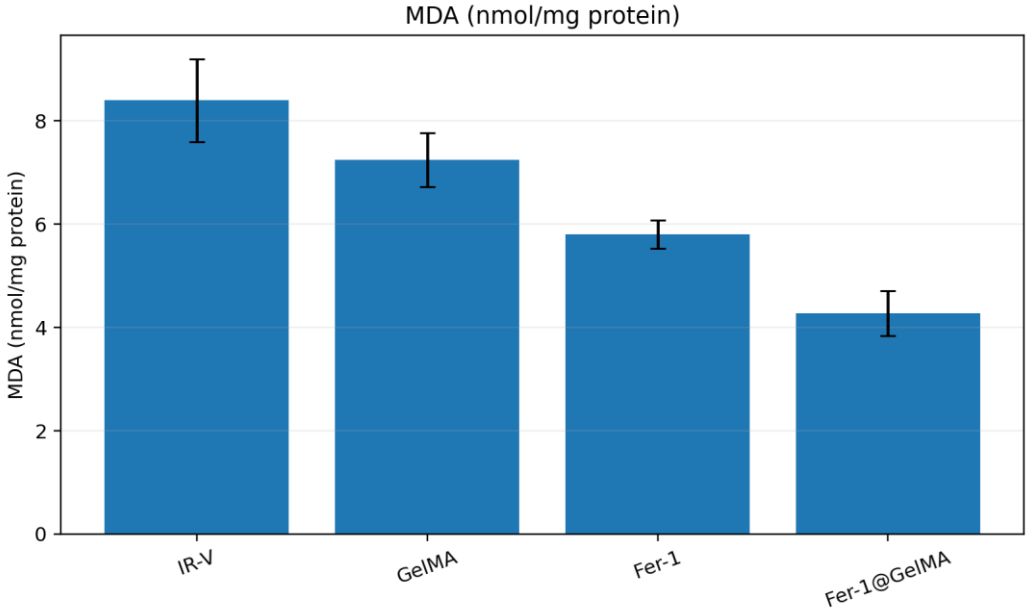


Figure 7. Tissue malondialdehyde on postoperative day 7

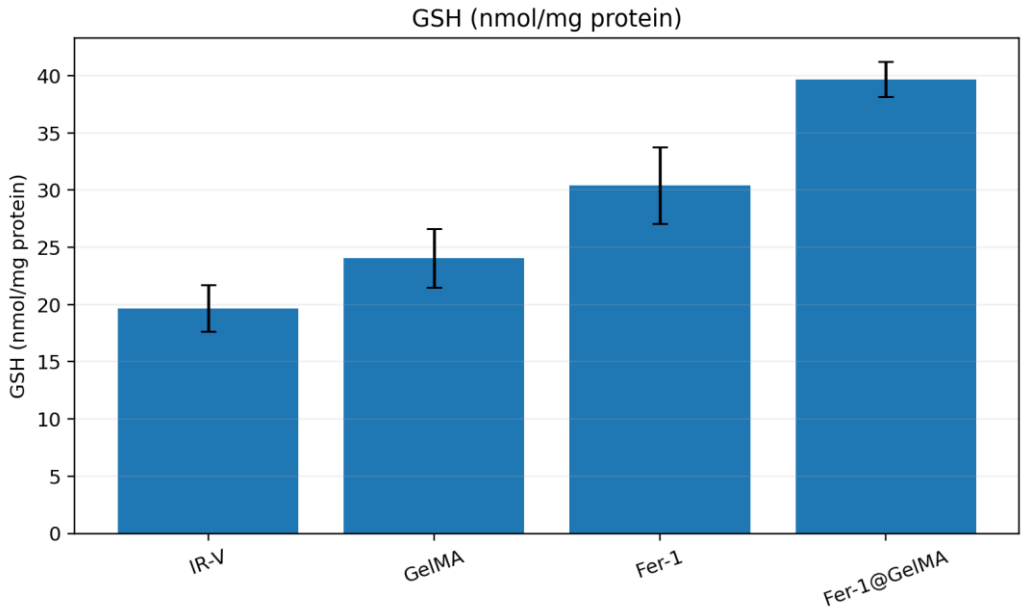


Figure 8. Tissue reduced glutathione on postoperative day 7

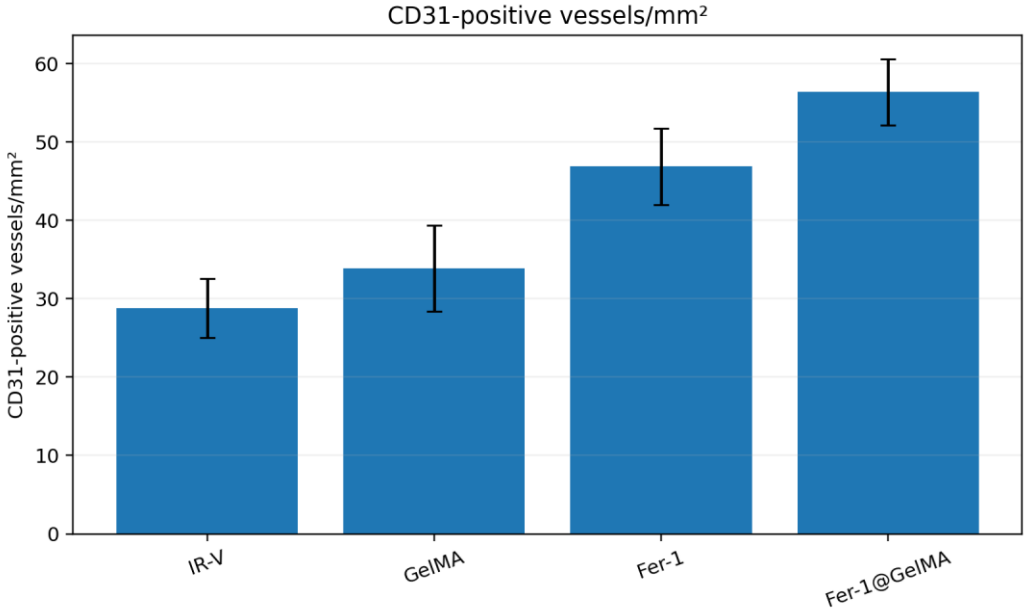


Figure 9. CD31-positive vessel density on postoperative day 7

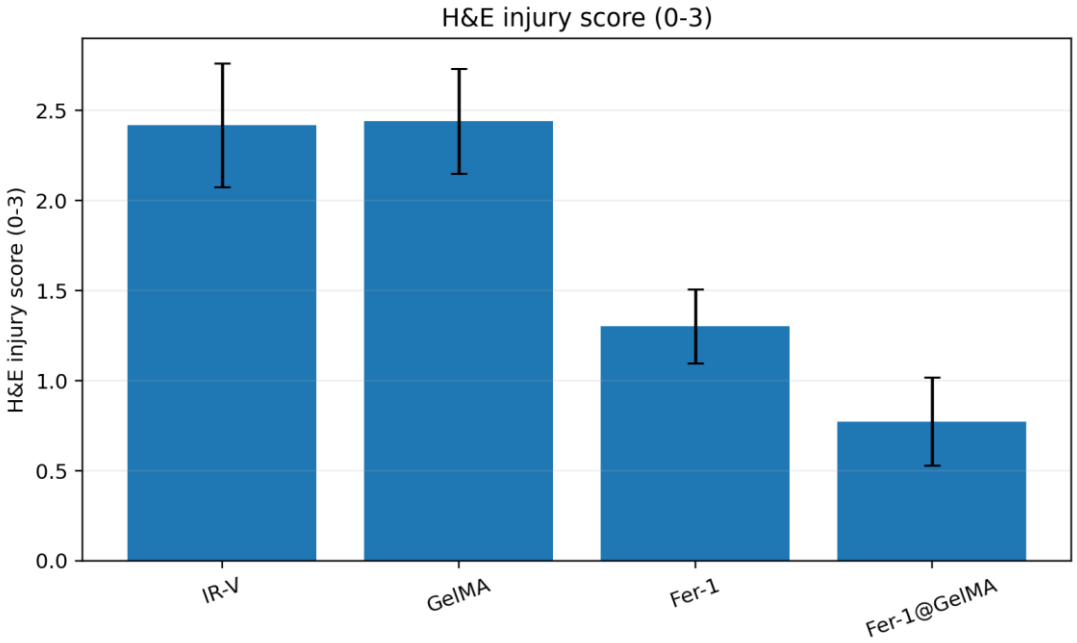


Figure 10. Composite H&E tissue-injury score on postoperative day 7

Discussion

Fer-1@GelMA produced the largest preservation of viable flap area and the strongest recovery of distal perfusion. The pattern was supported by independent biochemical, molecular and histologic endpoints: lower MDA, higher GSH, higher Nfe2l2 and Gpx4 expression, greater CD31-positive vascular density and less tissue injury [9], [10]. The convergence of these outcomes supports a ferroptosis-centered mechanism rather than a purely mechanical hydrogel effect.

Recent flap and wound studies have associated ferroptosis suppression with tissue preservation, including Nrf2/SLC7A11/GPX4 signaling and multiple hydrogel-based approaches. The present data extend that concept to a single local subflap depot of ferrostatin-1 [11], [12]. The free-drug group improved every major endpoint compared with vehicle, confirming pharmacologic activity; however, Fer-1@GelMA was consistently stronger, indicating that local retention during the early ischemic interval materially changed the response.

The molecular selection was deliberately narrow. Nfe2l2 represents upstream antioxidant transcriptional control and Gpx4 is a terminal phospholipid-hydroperoxide defense enzyme central to ferroptosis. Both were quantified with short published rat amplicons , while Gapdh was monitored as the reference transcript. The close alignment between Gpx4 expression, lower MDA and greater GSH provides biochemical support for the RT-qPCR findings [13], [14].

The GelMA-only group showed a modest improvement in survival and perfusion compared with vehicle. This likely reflects a favorable moist interface and matrix effect, but the much larger improvement with Fer-1@GelMA demonstrates that the drug component was necessary for the full response [15], [16]. The calibrated 405-nm crosslinking step is important for reproducibility because under-crosslinking could shorten retention whereas excessive light exposure could alter tissue response [17], [18].

The experiment has boundaries relevant to translation: only male rats were used, only one flap geometry and one ferrostatin-1 dose were evaluated, tissue drug concentration was not directly measured, and the endpoint was seven days. Future work should include dose-ranging, pharmacokinetic retention in the flap bed, female animals, tensile/mechanical assessment and longer remodeling endpoints before veterinary clinical evaluation.

Conclusion

A single local dose of ferrostatin-1 retained in photocrosslinked GelMA markedly improved random-pattern skin-flap viability, perfusion and microvascular density while reducing lipid peroxidation and strengthening Nfe2l2/Gpx4-associated antioxidant defense. The combination outperformed both blank GelMA and the same mass of free ferrostatin-1, supporting local ferroptosis inhibition as a promising reconstructive-surgery strategy.

References

[1] K. Tian and others, 'A deferoxamine-loaded microneedle patch enhances healing of radiation-induced skin injury: Potential involvement of ferroptosis', *ACS Applied Materials & Interfaces*, vol. 17, no. 10, pp. 15035–15049, 2025, doi: 10.1021/acsami.4c21589.

[2] C. Jin and others, 'A multifunctional hydrogel promotes diabetic wound healing by remodeling iron balance and energy metabolism', *Biomaterials*, vol. 326, p. 123640, 2026, doi: 10.1016/j.biomaterials.2025.123640.

[3] H. Zou and others, 'Bio-inspired supramolecular hydrogel inhibits ferroptosis to accelerate diabetic wound healing', *Journal of Advanced Research*, 2026, doi: 10.1016/j.jare.2026.01.024.

[4] Y. Chen and others, 'Cordycepin promotes the survival of random-pattern skin flaps via autophagy in a rat model', *Cellular Signalling*, vol. 134, p. 111890, 2025, doi: 10.1016/j.cellsig.2025.111890.

[5] E. S. Özden and others, 'Effects of tasimelteon treatment on traumatic brain injury through NRF-2/HO-1 and RIPK1/RIPK3/MLKL pathways in rats', *Molecular Neurobiology*, vol. 62, no. 10, pp. 12383–12392, 2025, doi: 10.1007/s12035-025-04711-0.

[6] X. Liu and others, 'Enhanced hydrogel loading of quercetin-loaded hollow mesoporous cerium dioxide nanoparticles for skin flap survival', *Materials Today Bio*, vol. 30, p. 101432, 2025, doi: 10.1016/j.mtbio.2024.101432.

[7] Z. Yang and others, 'Exploring the analgesic initiation mechanism of Tuina in the dorsal root ganglion of minor CCI rats via the TRPV1/TRPA1-cGMP pathway', *Pain Research and Management*, vol. 2024, p. 2437396, 2024, doi: 10.1155/2024/2437396.

[8] O. Akdemir, A. Eyuboglu, E. O. Cetin, and Y. Uyanikgil, 'Lutein protects ischemic skin flaps via antioxidant and anti-inflammatory mechanisms in a rat model of ischemia-reperfusion injury', *Journal of Investigative Surgery*, 2025, doi: 10.1080/08941939.2025.2528341.

[9] R. Du *et al.*, 'Mechanism of ferroptosis in a rat model of premature ovarian insufficiency induced by cisplatin', *Scientific Reports*, vol. 13, no. 1, p. 4463, 2023, doi: 10.1038/s41598-023-31712-7.

[10] C. Lin and others, 'MMP-9 responsive hydrogel promotes diabetic wound healing by suppressing ferroptosis of endothelial cells', *Bioactive Materials*, vol. 43, pp. 240–254, 2025, doi: 10.1016/j.bioactmat.2024.09.006.

[11] S. Jeon and others, 'Sustained oxygen-releasing hydrogel implants enhance flap regeneration by promoting mitochondrial biogenesis under mild hypoxia', *Bioactive Materials*, vol. 51, pp. 559–574, 2025, doi: 10.1016/j.bioactmat.2025.04.010.

[12] T. Wang, Y. Zheng, J. Zhang, and Z. Wu, 'Targeting ferroptosis promotes diabetic wound healing via Nrf2 activation', *Heliyon*, vol. 10, no. 19, p. e37477, 2024, doi: 10.1016/j.heliyon.2024.e37477.

[13] W. Xiong and others, 'PF-PEG@ASIV-EXO hydrogel accelerates diabetic wound healing by ferroptosis resistance and promoting angiogenesis', *ACS Biomaterials Science & Engineering*, vol. 10, no. 10, pp. 6263–6285, 2024, doi: 10.1021/acsbiomaterials.4c00692.

[14] H. Chen and others, 'Protective effects of the bioactive peptide from maggots against skin flap ischemia-reperfusion injury in rats', *Heliyon*, vol. 10, no. 9, p. e29874, 2024, doi: 10.1016/j.heliyon.2024.e29874.

[15] Y. Li and others, 'Remote ischemic preconditioning enhances skin flap survival via ZNF667/SDF1-mediated endothelial progenitor cells functions for angiogenesis', *Tissue Engineering and Regenerative Medicine*, vol. 23, no. 6, pp. 881–899, 2026, doi: 10.1007/s13770-026-00817-1.

[16] Z. Wang and others, 'Safranal accelerates diabetic wound healing by suppressing ferroptosis through modulation of transcription factor Forkhead Box O3', *Phytomedicine*, vol. 150, p. 157675, 2026, doi: 10.1016/j.phymed.2025.157675.

[17] W. Liu and others, 'Supermolecular poly-N-acryloyl glycinamide/polyglutamic acid/Fe3+ hydrogel incorporated with bioactive small extracellular vesicles promote diabetic wound healing by suppressing ferroptosis', *International Journal of Biological Macromolecules*, vol. 308, p. 142313, 2025, doi: 10.1016/j.ijbiomac.2025.142313.

[18] Y. C. Kim and others, 'Therapeutic potential of bovine colostrum-derived exosomes for ischemia-reperfusion injury in skin flaps: A rat model study', *Plastic and Reconstructive Surgery*, Jun. 2026, doi: 10.1097/PRS.0000000000013264.